Eur. Phys. J. B **39**, 27–33 (2004)
DOI: 10.1140/epjb/e2004-00166-1

THE EUROPEAN PHYSICAL JOURNAL B

Lattice dynamics and elastic properties of PbF_2 and BaF_2 from quantum mechanical calculations

A. Dubinin[1], B. Winkler[1,a], K. Knorr[2], and V. Milman[3]

[1] Mineralogisches Institut, Johann Wolfgang Goethe-Universität, Senckenberganlage 30, 60054 Frankfurt a.M., Germany
[2] Institut für Geowissenschaften/Kristallographie, Christian Albrechts Universität, Olshausenstr. 40, 24098 Kiel, Germany
[3] Accelrys, 334 Cambridge Science Park, Cambridge CB4 0WN, UK

Received 5 March 2004
Published online 18 June 2004 –

Abstract. The lattice dynamics of β-PbF_2, α-PbF_2 and cubic BaF_2 were studied using density-functional perturbation theory. These calculations show that the bonding in the two PbF_2 polymorphs is very similar. Phonon densities of states and heat capacities have been calculated and compared to the available experimental data. The results imply that anharmonicity begins to become significant already at temperatures as low as ∼100 K. The computed elastic stiffness coefficients of the PbF_2 polymorphs are used to discuss the unusual observation that the denser orthorhombic polymorph, thought to be the high pressure modification, is significantly more compressible than the cubic form.

PACS. 62.20.Dc Elasticity, elastic constants – 63.20.Dj Phonon states and bands, normal modes, and phonon dispersion – 65.40.Ba Heat capacity – 71.15.Nc Total energy and cohesive energy calculations

1 Introduction

Fluorides constitute a large family of compounds with interesting physical properties, crystallizing in a variety of structures [1–6]. Many of them are already employed in technological applications, such as e.g. optical coatings. Specifically, fluorides crystallizing in the fluorite structure have been studied extensively (see references in [7]). However, several open questions pertaining to structure-property relationships remain. The clarification of many of these will rely on atomistic model calculations, so we considered it worthwhile to complement the existing body of knowledge with a quantum mechanical study of PbF_2 and related BaF_2.

Cubic β-PbF_2 has attracted considerable attention as it becomes a superionic conductor at the relatively low temperature of 710 K [8]. The β-polymorph crystallizes in the fluorite-type structure with space group $Fm\bar{3}m$, cell parameter $a = 5.94$ Å and atomic positions (0, 0, 0) for Pb and ($\frac{1}{4}$, $\frac{1}{4}$, $\frac{1}{4}$) for F [1]. The orthorhombic α-polymorph crystallizes in the cotunnite type structure with space group *Pnma* and cell parameters $a = 6.440$ Å, $b = 3.899$ Å and $c = 7.651$ Å [2]. There has been a controversial discussion about the relative stability of the α- and β-polymorph at ambient conditions. Using a Pb/β-PbF_2//KF(aq)//α-PbF_2/Pb electrochemical cell, Kennedy et al. [9] measured an open circuit potential of +1.7 mV, indicating that the β form is more stable by ∼0.33 kJ/mol. However, this conclusion has been questioned on the basis of high-pressure differential thermal analysis (DTA) [10] and elastic constants data [11]. Volodkovich et al. [12] considered the α-phase to be thermodynamically stable and the β-phase being metastable at room temperature. However, the basis for this point of view was not elucidated. Hence, additional information with respect to the relative stability is of interest, and here quantum mechanical model calculations have been used to discuss the contribution of the lattice energies.

Interatomic interactions can be studied by investigating the lattice dynamics. Phonon dispersion curves of β-PbF_2 were determined by coherent inelastic neutron scattering at 10 K [13] and, with the exception of the optic phonon with the highest frequency, the lattice dynamics of this compound are therefore well-known. The phonon density of states has been constructed from the experimental data by fitting a core-shell model to the phonon dispersion curves [13]. As a result of the lack of measurements at high frequencies, the reliability of the core-shell model for this part of the spectrum is questionable, and the rather steep dispersion of the highest frequency optic branch in the [ξξξ]-direction predicted by the core-shell model calculations remains to be verified. Quantum mechanical calculations can be employed to compute phonon

[a] e-mail: b.winkler@kristall.uni-frankfurt.de

dispersion relations [14], and here the lattice dynamics and the thermodynamic properties of β-PbF_2 in the harmonic approximation are discussed.

The computed thermodynamic properties can be compared to experimentally determined heat capacity data. At low temperatures between 3 and 22 K one data set was presented [15], while two data sets were obtained at higher temperatures [12,16]. They are in rather poor agreement with each other.

The elastic stiffness coefficients of crystals reflect the dominating interatomic interactions. For β-PbF_2, all components of the elastic tensor c_{ij} were determined experimentally [11,17], while for the α-phase only the bulk modulus was obtained from compression measurements [18].

To further evaluate the results obtained for β-PbF_2, the isostructural cubic compound BaF_2, which becomes superionic at significantly higher temperatures $\approx$1300 K [19], was studied. In particular BaF_2 has been chosen since reliable experimental data are available. Its lattice dynamics was studied in detail [20] and the specific heat was measured in the temperature region from 3 to 300 K [21,22].

2 Computational details

The quantum mechanical calculations performed here are based on density functional theory, DFT. While DFT itself is exact [23,24], practical calculations require an approximation for the treatment of the exchange and correlation energies. Here the well-established local density approximation (LDA) [24] and the generalized gradient approximation (GGA) [25] were used. Full geometry optimizations of structures with several structural degrees of freedom are most efficiently performed if the stress tensor for a given configuration can be evaluated, which is most straightforward in the computational approaches that use a basis set of plane waves to represent the charge density and electronic wavefunctions. However, as it is impractical to consider tightly bound core electrons explicitly when using a plane-wave basis set, pseudopotentials have to be used to mimic the screening of the Coulomb potential of the nucleus by the core electrons. A number of approaches for the construction of pseudopotentials have been presented in the literature [26,27]. Here, norm-conserving and ultrasoft pseudopotentials [28,29] have been used. The former are required for 'linear response' calculations, for which an implementation with ultrasoft pseudopotentials is not yet available, while the computationally more efficient ultrasoft pseudopotentials have been used to study elastic stiffness coefficients.

Lattice dynamics calculations of cubic BaF_2, β- and α-PbF_2 have been performed using the ABINIT (v. 3.4.3) pseudopotential plane-wave code [30]. We used norm-conserving pseudopotentials taken from the ABINIT data base. For Ba and Pb we used the 'Teter extended norm-conserving' pseudopotentials, and for F the norm-conserving Troullier-Martins pseudopotential [31]. Based on convergence studies we chose a cutoff energy of 80 Ha as the cutoff energy for the PbF_2-polymorphs. In addition to the cutoff energy, only one further parameter determines the quality of the calculations, namely the density of points with which the Brillouin zone is sampled. For β-PbF_2 we used a $4\times4\times4$ k-point grid without shifts. This corresponds to 8 k-points for the unperturbed structure, and 64 k-points for the calculation of the perturbed structure, necessary to obtain the complete dynamical matrix. For the ground state calculations of α-PbF_2 a $2\times4\times2$ k-point grid without shifts was employed. For the calculations of BaF_2 a cutoff energy of 50 Ha and a $2\times2\times2$ k-point grid with 4 shifts were used. This k-point grid results in 2 k-points for the unperturbed structure and 32 k-points for the perturbed one.

Table 1. Comparison of measured and calculated cell parameters of the two PbF_2-polymorphs and cubic BaF_2. Experimental cell parameters and densities for α-PbF_2 are taken from [1,2], for β-PbF_2 from [1] and for cubic BaF_2 from [33].

Compound		Exp.	DFT-LDA	DFT-GGA
α-PbF_2	a [Å]	6.44	6.314	6.599
	b [Å]	3.899	3.812	3.968
	c [Å]	7.651	7.558	7.851
	density [g/cm^3]	8.45	8.96	7.93
β-PbF_2	a [Å]	5.943	5.832	6.029
	density [g/cm^3]	7.75	8.21	7.45
BaF_2	a [Å]	6.196	6.095	6.261
	density [g/cm^3]	4.89	5.15	4.75

Elastic stiffness coefficients of PbF_2 have been calculated using the pseudopotential plane-wave code CASTEP [32] with ultrasoft pseudopotentials from the CASTEP database. The calculation of elastic constants is based on applying small strains to the ground state structure, followed by relaxation of the atomic positions and a subsequent computation of the stress tensor. Elastic coefficients were determined from a linear fit of the computed stress to the applied strain, where 6 strain amplitudes up to a maximum of 0.003 have been used. A cutoff energy of 13.6 Ha and 24 k-points have been used.

3 Results and discussion

The cell parameters obtained from the ground state calculations of the two PbF_2-polymorphs and cubic BaF_2 are listed in Table 1. They are in a good agreement with experimental data [1,2,33]. As expected, the LDA-calculations show the effect of overbinding and give lattice parameters too small by 2%, while the GGA calculations give lattice parameters too large by 2%. From these calculations, the β-phase is more stable by 2−7 kJ/mol, depending on the pseudopotentials and the exchange-correlation functional used.

The elastic stiffness tensor c_{ij} (in Voigt's notation) of cubic crystals has three independent components, c_{11}, c_{12}

Table 2. Comparison between elastic stiffness coefficients of β-PbF_2 obtained from DFT-GGA calculations, experimentally determined values at ambient temperature, experimental values extrapolated to low temperatures and those obtained from the core-shell model calculations, where the parameters have been fitted to phonon dispersion curves obtained at 10 K.

	Calc. DFT (athermal)	Exp. ultrasound at RT [11,17]	Extrapolated to 0 K from [17]	Exp. from phonons at 10 K [13]
c_{11} [GPa]	105	96	115	105−119
c_{12} [GPa]	52	47	57	49−64
c_{44} [GPa]	27.8	21	22	23.6−24.5

and c_{44}. The calculated components of the elastic stiffness tensor of β-PbF_2 are compared to data obtained from ultrasound spectroscopy [17] after extrapolation to low temperatures (Tab. 2).

This extrapolation to low temperatures is required, as the elastic stiffness constants were calculated in the athermal limit and the experimental data show a significant temperature dependence. For the comparison of the results obtained here with those from earlier core-shell model calculations such an extrapolation was not necessary, since the core-shell model was derived from phonon measurements at 10 K [13]. The agreement between the core-shell model calculations and the DFT-based calculations is good, the largest discrepancy is 10% for c_{44}. With the exception of c_{44}, the values computed here are between the values obtained at 300 K from ultrasound experiments and those extrapolated to 0 K linearly. This most probably suggests that the temperature derivative of the thermal expansion coefficient is not a constant over the whole range, and that at low temperatures the temperature-induced change of the thermal expansion is smaller than at high temperatures. The 20% disagreement between the value of c_{44} determined by ultrasonic measurements and the theoretical value obtained here is most probably due to a frequently observed systematic overestimation of the covalent bonding in DFT-calculations [34].

A comparison of the computed to the experimentally determined bulk modulus again shows the influence of temperature. The bulk modulus, b_0, can be calculated from the elastic compliance matrix, s_{ij}, which is reciprocal to the elastic stiffness matrix, i.e. $(s_{ij}) = (c_{ij})^{-1}$, so that

$$K_T = \frac{1}{b_0} = \sum_{i=1}^{3}\sum_{j=1}^{3} s_{ij}, \qquad (1)$$

where K_T is the isothermal compressibility. The calculated b_0 from the elastic constants is 69.7 GPa, in between the value calculated from the elastic constants measured at room temperature ($b_{0,300\mathrm{K}} = 63.2$ GPa) and the b_0 obtained from elastic constants extrapolated to 0 K, $b_{0,0\mathrm{K}} = 76.3$ GPa (see Tab. 2). The value we obtained for the bulk modulus is similar to a gradient-corrected full-potential linear muffin-tin orbital calculation [35], where a value of $b_0 = 71$ GPa was obtained, while a Hartree-Fock based study [36] obtained a significantly lower value of 56 GPa.

We also have predicted the elastic stiffness tensor for α-PbF_2. The computed values for the c_{ij} are (in GPa): $c_{11} = 87$, $c_{22} = 103$, $c_{33} = 93$, $c_{44} = 20$, $c_{55} = 23$, $c_{66} = 27$, $c_{12} = 47$, $c_{13} = 46$, and $c_{23} = 50$. The numerical errors associated with each components are about 5%. These components have not been determined experimentally, as this would require a large single crystal. However, the bulk modulus has been obtained from an X-ray high-pressure study, where an isothermal equation of state gave $b_0 = 47.0(6)$ GPa at room temperature [18]. This value is more reliable than a value of 117(4) GPa obtained earlier in a restricted pressure range [8]. We obtained a bulk modulus of $b_0 = 63$ GPa. Again, a significant part of the discrepancy will be due to the neglect of the influence of temperature in the present study. However, both experimental measurements and quantum mechanical models show unambiguously that the orthorhombic α-PbF_2 is denser by 6% then the β-phase. Usually the compressibility of the denser polymorph is smaller. This would not necessarily be the case if the compression mechanism of the high pressure form was significantly different from that of the low pressure form. The compression mechanism of the α-phase has been studied experimentally [18]. While in the cubic polymorph compression does not change the relative atomic arrangement, pressure increase leads to a distortion of the coordination polyhedron in the α-phase. The latter compression mechanism seems to be energetically much more favorable and hence the bulk modulus of α-PbF_2 is smaller than that of β-PbF_2, despite the α-polymorph being denser. If we assume that the temperature dependence of b is similar for the two polymorphs, then the agreement between the value computed here (63 GPa) and the experimental value extrapolated to 0 K (≈56 GPa) is satisfactory also for α-PbF_2.

The results of the lattice dynamics calculations for the cubic polymorphs of PbF_2 and BaF_2 are shown in Figures 1 and 2, where they are compared to neutron scattering data. Our calculations reproduce the experimentally determined phonon dispersion curves with the accuracy expected from DFT-LDA linear response calculations. For calculations of the phonon frequencies at the Γ-point the coupling between atomic displacements and the electric field has to be taken into account. This interaction causes a splitting between the longitudinal and transverse optic modes at the Γ-point, the so-called LO-TO splitting. The computation of the value of LO-TO splitting is based on

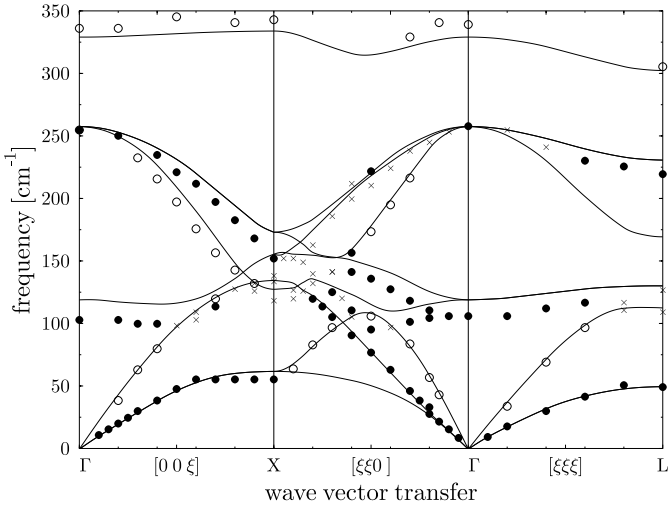

Fig. 1. Measured (at 10 K) and calculated (lines) phonon dispersion relations for β-PbF_2 in three high symmetry directions. Closed (open) circles are predominantly transverse (longitudinal) modes. The crosses represent observed points for which a symmetry assignment was not possible [13].

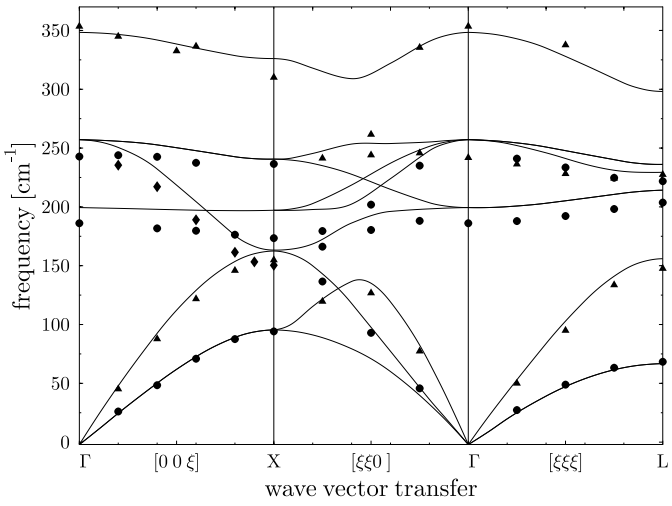

Fig. 2. Measured (at 300 K) and calculated (lines) phonon dispersion relations for BaF_2 in three high symmetry directions. Different point symbols correspond to the different group representation of the measured phonons [20].

the computation of the Born effective charges, which we obtained to be 3.24 and $-1.62e$ for Pb and F, respectively. The calculated LO-TO splitting in β-PbF_2 is 211 cm^{-1}.

For β-PbF_2 our calculations clearly indicate that the highest optic branch remains nearly dispersionless in the [ξξξ]-direction, in contrast to the prediction of the earlier core-shell model calculations [13]. The highest frequency optic branch remains also nearly dispersionless in the other directions. This is also evident in the density of states (Fig. 3), where the quantum mechanical model gives a much more localized distribution over 60 cm^{-1} in

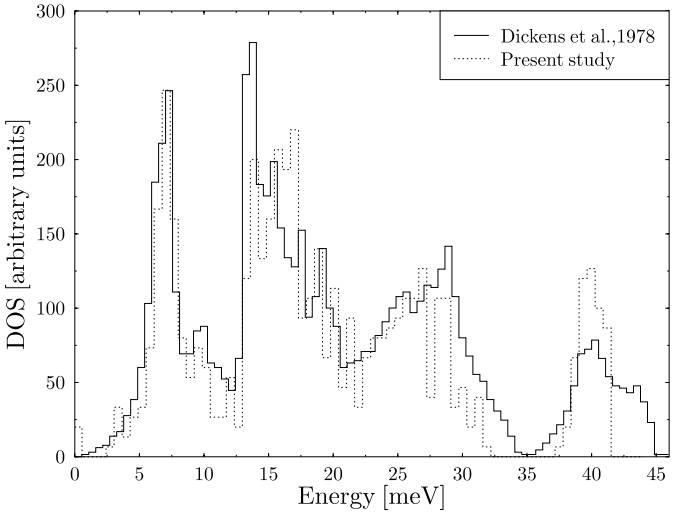

Fig. 3. Phonon density of states of cubic PbF_2. The solid line represents a density of states derived from empirical model calculations, where the parameters had been fitted to coherent inelastic neutron scattering data [13]. The DOS given by the dashed line has been obtained from linear response calculations.

the high frequency region then the core-shell model calculations. This high frequency phonon is dominated by the dynamics of the light fluorine ions, and hence the current results indicate a comparatively weak bonding of the fluorine ions to the cation sublattice and, subsequently, a weak correlation between the dynamics of individual fluorine ions. In isostructural CaF_2 for example, the same phonon is at 330−470 cm^{-1} [37], i.e. it has a significantly higher energy and a dispersion twice as large as in PbF_2. This is due to the fact that the cation-anion bond in CaF_2 is much stronger than in PbF_2 and the dynamics of the anions displays a larger degree of correlation.

Because of the lower symmetry of α-PbF_2, the analogous calculations require significantly more computational resources. As no large single crystals are available it is unlikely that full phonon dispersion curves will be determined experimentally, and hence we restricted the calculations to a set of 4 k-points, which is sufficient to demonstrate that the phonon frequencies in the two polymorphs are very similar. In both cases a high frequency regime from 300−360 cm^{-1} is separated by a gap from a low frequency regime from 0−260 cm^{-1}. Hence, the bonding in the two polymorphs is very similar as well.

The specific heat at constant volume, C_V, of β-PbF_2 (Fig. 4) has been calculated from the density of states. For comparing to experimental data, C_V has to be converted to specific heat at constant pressure, C_P. Within the harmonic approximation the relation between the molar specific heat capacities C_V and C_P is expressed by the formula:

$$C_P = C_V + TV\beta^2/K_T, \qquad (2)$$

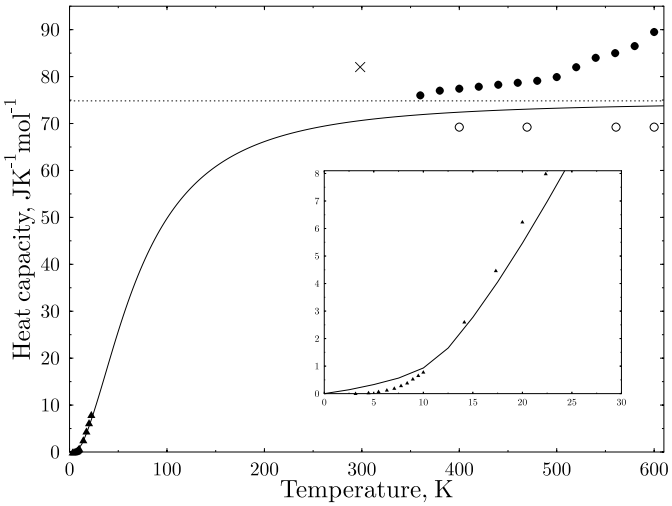

Fig. 4. Experimentally determined and calculated specific heat of cubic PbF_2. The low-temperature data have been measured by [15] (full triangles). The high-temperature data have been measured by [16] (open circles) and by [12] (full circles). The cross represents the room temperature (298 K) specific heat obtained as a slope of the high temperature heat content, which is linear up to about 600 K [38].

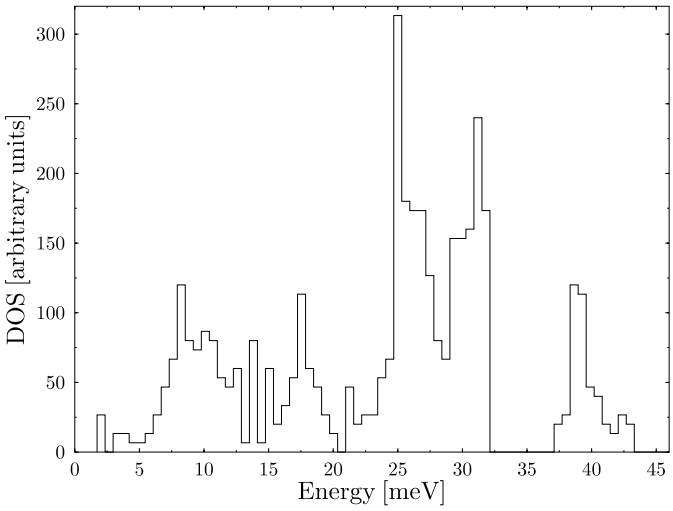

Fig. 5. Calculated phonon density of states of cubic BaF_2.

where V is the molar volume, β is the thermal expansion coefficient and K_T is the isothermal compressibility. For β-PbF_2, the molar volume $V = 31.6$ cm^3/mol, $K_T = 1/b_0 = 0.0159$ GPa^{-1}, where the bulk modulus b_0 (at 300 K) has been calculated from the elastic constants obtained from ultrasonic measurements [17] and the thermal expansion coefficient was taken to be $\beta(T) = 2.73 \times 10^{-6} + 7.03 \times 10^{-8}T$ [17]. This implies that within the investigated temperature range the maximal difference between C_V and C_P is 1.2 J mol^{-1} K^{-1} at high temperatures, and hence can be neglected.

At low temperatures ($T < 25$ K), the theoretical values for the heat capacity agree with experimentally determined ones to within 0.5 J mol^{-1} K^{-1}. This is sufficient for most investigations. Probably an even better sampling of reciprocal space would improve the agreement, as a comparison with experiment shows an initial overestimation of C_P, indicative of an overestimation of the influence of the acoustic phonons. At high temperatures, C_V calculated in the harmonic approximation will approach the limiting Dulong-Petit value of $9R$. Two experimentally determined data sets for the high-temperatures region differ significantly [12,16]. In fact, the values by [16] are smaller than the ones we calculated here, which indicates a measurement error, as the calculations in the harmonic approximation on an ideal defect free crystal present a lower boundary. A value for the room temperature C_P, derived as a slope of the high temperature heat content, seems to be far too large [38]. A comparison to the data of [12] allows to compute the influence of anharmonicity, which is about 5 J mol^{-1} K^{-1} at 350 K. Regrettably, no data is currently available for the intermediate temperature region.

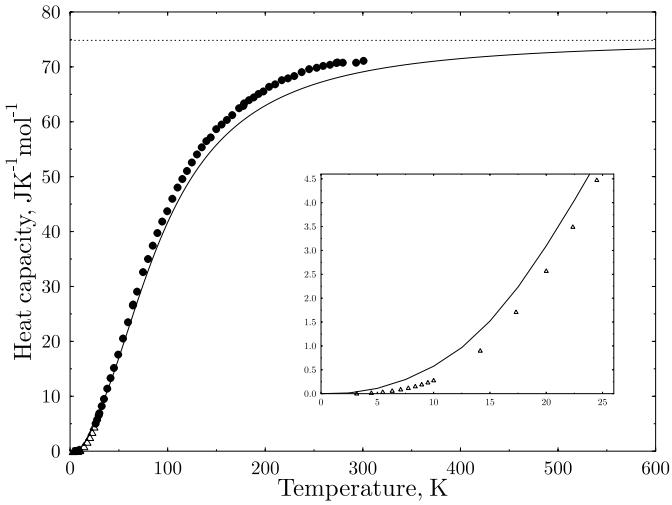

Fig. 6. Computed specific heat (line) of BaF_2 is compared to measured between 3 and 25 K specific heat data [21] (open triangles) and the data measured from 25 to 300 K [22] (full circles).

Similar calculations as those described above have been performed for cubic BaF_2 (Figs. 5 and 6). The values of the Born effective charges are 2.61 and $-1.30e$ for Ba and F, respectively. The corresponding value of the LO-TO splitting is 149 cm^{-1}. The dispersion of the highest frequency optic mode is about 100 cm^{-1}, in between the value of PbF_2 and CaF_2. Experimentally obtained specific heat data are available from low temperatures up to 300 K and are compared to the data obtained from the density of states in Figure 6. A similar calculation as presented above for β-PbF_2 shows that the difference between C_V and C_P is negligible. The comparison shows that the error due to a too coarse sampling of reciprocal space, slightly inaccurate phonon frequencies, the neglect of defects and the influence of temperature etc. is again of the order of

1 J mol^{-1} K^{-1}. At 300 K the experimental and the theoretical values differ by 2−3 J mol^{-1} K^{-1}, which is similar to what an extrapolation would give in the case of β-PbF_2.

4 Conclusions

The current calculations have shown, that in the athermal limit the ground state structure of PbF_2 is the cubic polymorph. The lattice dynamics, and hence the entropic contribution to the Gibbs free energy in the harmonic approximation, are very similar for the two polymorphs. Therefore, more extensive accurate calculations, especially for α-PbF_2, are required to make quantitative predictions of the relative stability of the polymorphs.

Our calculations of the heat capacities show that at low temperatures the current approach reproduces the experimental values of heat capacities to within 0.5 J mol^{-1} K^{-1}. Noticeable deviations from the harmonic approximation are evident for BaF_2 already at rather low temperatures of 100 K. Although we are not aware of heat capacity data for β-PbF_2 between 22 K and 360 K, the similarity to BaF_2 allows to confidently interpolate between the available data sets, and this would then imply that anharmonicity becomes noticeable in β-PbF_2 also at rather low temperatures of 100 K.

The difference between the lattice dynamics of PbF_2 and BaF_2 is small, and for the low lying phonons it is due to the mass difference between Ba and Pb. This is confirmed by the simple comparison of the frequencies in the X-point of the Brilloiun zone:

$$\frac{\omega_{\mathrm{Ba}}}{\omega_{\mathrm{Pb}}} = \sqrt{\frac{M_{\mathrm{Pb}}}{M_{\mathrm{Ba}}}} \tag{3}$$

where ω_{Pb}, ω_{Ba} are frequencies in the X-point of the Brillouin zone, and M_{Pb}, M_{Ba} are atomic masses of Pb and Ba respectively. Frequencies at the X-point are compared because this corresponds to the lattice dynamics of planes with two different masses stacked along the direction [100]. Then, the frequency of the lowest optic branch is inversely proportional to the square root of the mass of the cation. In our case $\omega_{\mathrm{Pb}} = 155$ cm^{-1} and $\omega_{\mathrm{Ba}} = 197$ cm^{-1}. Atomic masses of Pb and Ba are 207.20 and 137.33 respectively. Substituting these numbers into equation (3) yields an agreement between the two sides within 3.4%, which again shows that the exchange of Pb with Ba does not alter the character of the bonding significantly. To illuminate the effect where a substitution does change the bonding, we compare our results to the lattice dynamics of CaF_2. The frequency ω_{Ca} at the X-point of the corresponding optic branch for CaF_2 is equal to 190 cm^{-1} [37] and the atomic mass of Ca is 40.08. Substitution of frequency ω_{Ca} and mass M_{Ca} instead of ω_{Ba} and M_{Ba} in the relation (3) gives a factor of nearly two between the left and right hand side of equation (3).

Of the three fluorides compared here, CaF_2 has the highest transition temperature into the superionic conducting phase of 1370 K [39]. This is not very much higher than the transition temperature of 1300 K reported for BaF_2 [19], while PbF_2 becomes superionic conducting at much lower temperatures (710 K) [8]. However, it seems that none of the physical properties studied here is correlated with the significant differences in these transition temperatures.

We are grateful to the Deutsche Forschungsgemeinschaft for financial support through project Wi 1232/13-1. The calculations have partially been performed using resources of the Center for Scientific Computing of the Johann Wolfgang Goethe University (Frankfurt a.M.). We are grateful for additional computer resources due to the support of Hewlett-Packard. We are also grateful to the ABINIT group for making their code publicly available.

References

1. K.F. Portella, K.R. Rattmann, G.P. De Souza, C.M. Garcia, M.P. Cantão, R Muccillo, J. Mat. Sci. **35**, 3263 (2000)
2. P. Boldrini, B.O. Loopstra, Acta Crystall. **22**, 744 (1967)
3. E. Morris, T. Groy, K. Leineweber, J. Phys. Chem. Sol. **62**, 1117 (2001)
4. C. Benoit, J. Giordano, J. Phys. C **21**, 5209 (1988)
5. W. Hayes, Contemp. Phys. **19**(5), 469 (1978)
6. W. Bollmann, Cryst. Res. Technol. **16**, 1039 (1981)
7. M. Mérawa, M. Llunell, R. Orlando, M. Gelize-Duvignau, R. Dovesi, Chem. Phys. Lett. **368**, 7 (2003)
8. S. Hull, D.A. Keen, Phys. Rev. B **58**, 14837 (1998)
9. J.H. Kennedy, R. Miles, J. Hunter, J. Electrochem. Soc. **120**(11), 1441 (1973)
10. W. Klement, L. Cohen, J. Electrochem. Soc. **126**(8), 1403 (1979)
11. J.C. Jamieson, M.H. Manghnani, T. Matsui, L.C. Ming, J. Geophys. Res. - Sol. Earth Plan. **91**(B5), 4643 (1986)
12. L.M. Volodkovich, G.S. Petrov, R.A. Vecher, A.A. Vecher, Thermochimica Acta **88**, 497 (1985)
13. M.H. Dickens, M.T. Hutchings, J. Phys. C **11**, 461 (1978)
14. S. Baroni, S. de Gironcoli, A.D. Corso, P. Giannozzi, Rev. Mod. Phys. **73**, 515 (2001)
15. D.P. Dandekar, J.J. Tsou, J.C. Ho, Phys. Rev. B **20**, 3523 (1979)
16. D.S. Rimai, R.J. Sladek, Solid State Commun. **31**, 473 (1979)
17. M.O. Manasreh, D.O. Pederson, Phys. Rev. B **30**, 3482 (1984)
18. L. Ehm, K. Knorr, F. Mädler, H. Voigtländer, E. Busetto, A. Cassetta, A. Lausi, B. Winkler, J. Phys. Chem. Sol. **64**, 919 (2003)
19. M.F. Butman, A.A. Smirnov, L.S. Kudin, H. Dabringhaus, Surf. Sci. **489**, 983 (2001)
20. J.P. Hurrell, V.J. Minkiewicz, Solid State Commun. **8**, 463 (1970)
21. D.P. Dandekar, J. Fontanella, C.H. Huoh, J.C. Ho, Phys. Rev. B **26**, 2264 (1982)
22. K.S. Pitzer, W.V. Smith, W.M. Latimer, J. Am. Chem. Soc. **60**, 1826 (1938)
23. P. Hohenberg, W. Kohn, Phys. Rev. **136**(3B), 864B (1964)
24. W. Kohn, L.J. Sham, Phys. Rev. **140**(4A), 1133A (1965)
25. J.A. White, D.M. Bird, Phys. Rev. B **50**, 4954 (1994)

26. G.B. Bachelet, D.R. Hamann, M. Schlüter, Phys. Rev. B **26**, 4199 (1982)
27. L. Kleinman, D.M. Bylander, Phys. Rev. Lett. **48**, 1425 (1982)
28. D. Vanderbilt, Phys. Rev. B **41**, 7892 (1990)
29. C. Lee, D. Vanderbilt, K. Laasonen, R. Car, M. Parrinello, Phys. Rev. B **47**, 4863 (1993)
30. X. Gonze, J.-M. Beuken, R. Caracas, F. Detraux, M. Fuchs, G.-M. Rignanese, L. Sindic, M. Verstraete, G. Zerah, M. Jollet, F. Torrent, A. Roy, M. Mikami, Ph. Ghosez, J.-Y. Raty, D.C. Allan, Comput. Mat. Sci. **25**, 478 (2002)
31. `http://www.abinit.org/`
32. S.J. Clark, M.D. Segall, P.J.D. Lindan, M.J. Probert, C.J. Pickard, P.J. Hasnip, M.C. Payne, J. Phys.: Condens. Matt. **14**, 2717 (2002)
33. A.S. Radtke, G.E Brown, Am. Mineralogist **59**, 885 (1974)
34. B. Winkler, M. Hytha, M.C. Warren, V. Milman, J.D. Gale, J. Schreuer, Z. Kristallogr. **216**, 67 (2001)
35. H.E. Lorenzana, J.E. Klepeis, M.J. Lipp, W.J. Evans, H.B. Radousky, M. van Schilfgaarde, Phys. Rev. B **56**, 543 (1997)
36. A. Costales, M.A. Blanco, R. Pandey, J.M. Recio, Phys. Rev. B **61**, 11359 (2000)
37. M.M. Elcombe, A.W. Pryor, J. Phys. C **3**, 492 (1970)
38. C.E. Derrington, A. Navrotsky, M. O'Keeffe, Solid State Commun. **18**, 47 (1976)
39. B.M. Voronin, S.V. Volkov, J. Phys. Chem. Sol. **62**, 1349 (2001)